Eur. Phys. J. D (2015) 69: 259
DOI: 10.1140/epjd/e2015-60378-x

THE EUROPEAN PHYSICAL JOURNAL D

Regular Article

Measuring high pressure equation of state of polystyrene using laser driven shock wave

Hua Shu[a], Xiuguang Huang, Junjian Ye, Jiang Wu, Guo Jia, Zhiheng Fang, Zhiyong Xie, Huazhen Zhou, and Sizu Fu

Shanghai Institute of Laser Plasma, Shanghai 201800, P.R. China

Received 26 June 2015 / Received in final form 24 August 2015
Published online 24 November 2015 –

Abstract. High precision polystyrene equation of state data were measured using laser-driven shock waves with pressures from 180 GPa to 700 GPa. α quartz was used as standard material, the shock wave trajectory in quartz and polystyrene was measured using the Velocity Interferometer for Any Reflector (VISAR). Instantaneous shock velocity in quartz and polystyrene was obtained when the shock wave pass the interface. This provided ∼1% precision in shock velocity measurements.

1 Introduction

Equation of state (EOS) data of matter in high pressure regime is a subject of interest for many fields of modern physics [1–3], including astrophysics, geophysics. In particular, in the inertial confinement fusion (ICF) [4–6] researches, compression efficiency and shock structure in fusion capsules critically depend on the EOS. In the past, TPa pressures can be achieved by strong shock waves driven with high-energy pulse powers such as nuclear explosions [7–9]. Recently, laser-driven shock waves provided equation of state (EOS) data for a variety of materials used in high-energy-density physics experiments at pressures above 1 Mbar. Polystyrene (CH) is suggested as ablators for inertial confiment fusion (ICF) capsules. Understanding how Polystyrene and plastic foams ablators [10–14] respond to several Mbar shock waves is critical to optimizing ICF target performance.

In this paper, laser-driven shock waves were used to produce high-precision impedance-matching measurements using quartz as a reference material. This provided ∼1% precision in shock velocity measurements. High precision polystyrene equation of state data were obtained using laser-driven shock waves with pressures from 180 GPa to 700 Gpa.

2 Experiment setup

The experiment was performed using the "SG-II" Nd: Glass laser (converted at $\lambda = 0.527$ μm) of the National Laboratory on High Power Laser and Physics. The "Shenguang-II" Laser facility provides one-dimensional compression by smoothed laser beams with short wavelength and high intensity. The temporal profile of the laser is nearly square with a rise and fall time of ∼300 ps and a full width at half maximum (FWHM) of ∼3 ns. Lens-array (LA) [15,16] was used to eliminate the large scale spatial modulation and to obtain a flat-topped profile in the focal plane. Characteristics of the optical system (Lens + LA) were such that the focal spot had a flat region of either ∼1 mm or ∼0.4 mm. The average laser intensity in the focal spot was between $0.5-2\times10^{14}$ W/cm^2.

The targets consisted of 50 μm α-quartz pushers with the samples mounted on the rear side. The sample were 47-μm-thick CH foils. Impedance measurements were performed at the interface between the quartz and the sample.

All targets had a 30 μm aluminum ablator (on the laser side) to absorb the incident laser and avoid shinethrough laser. To form a good initial interference and balance the probe laser intensity before and after shot (the reflection index of Cr is ∼30%, which is close to the reflection index of the shock front in quartz and CH.), the front side of quartz had a Cr reflective coating (200 nm thick). To minimize ghost reflections, the quartz and the sample had antireflection coatings. Material densities were 2.65 g/cm^3 for quartz, 1.05 g/cm^3 for CH. The indices of refraction for these materials at 660 nm probe laser wavelength were 1.54 and 1.59 for quartz and CH, respectively.

The principal diagnostic was a two-channel line-imaging velocity interferometer system for any reflector (VISAR) [17–19]. The shock velocities in the samples were measured using the VISAR. The laser drive strengths were strong enough to produce optically reflective shock fronts in both the quartz and polystyrene samples. This resulted

[a] e-mail: shuhua_79@hotmail.com

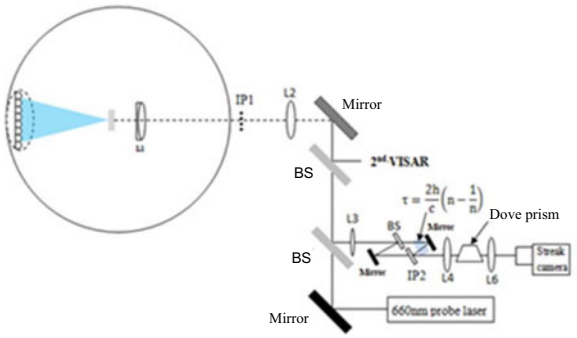

Fig. 1. Experimental setup in the SG-II laser facility.

in direct, time-resolved measurement of the shock speed in both the quartz and the CH samples. Two VISARs with different velocity sensitivities were used to discern the 2π phase-shift ambiguity that occurs when the shock speed instantaneously jumps at material interfaces. Etalons with 10 mm and 30 mm thicknesses were used to produce uncorrected velocity sensitivities of 5.63 and 1.88 km/s fringe, respectively. The indices of refraction determined the VISAR sensitivity in each material. The VISAR data were analyzed with a fast Fourier transform (FFT) method that establishs fringe position to ∼5% of a finge. Since the shock velocities used in these experiments usually lead to approximately five fringe shifts, velocities are measured to ∼1% precision. The probe laser for VISAR was a Q-switched laser operating at 660 nm with a pulse length of 60 ns at full width at half maximum (FWHM). The reflected probe signal was recorded by a visible streak camera. The temporal windows for each VISAR is either 20 or 10 ns. The response time of the diagnostic was controled by the delay time related to the etalons ∼170 ps or 60 ps.

The experimental setup is shown in Figure 1. The ninth beam of the "SG-II" Laser system irradiates the aluminum on the front of the targets, driving a strong shock that passes through the quartz and sample. The rear side of the target was viewed by VISAR, and since each of these layers is transparent, they measure the shock speed inside each layer. Figure 2b shows a typical VISAR data. The horizontal lines are the VISAR fringes, and its vertical position is proportional to the shock speed. Before $t = 1.0$ ns, the finges are horizontal and constant because the shock wave has not present. At $t = 3.0$ ns, the shock wave enters the quartz, where the VISAR catchs it. The shock wave strength decays as it propagates in the quartz. At $t = 6.0$ ns, the shock wave passes through the quartz-CH boundary and enters the CH sample, where its velocity changes. This is shown as the position of the VISAR fringes is jumped and there intensity has an abrupt change. The latter is caused by the difference in the reflectivities of the shock waves in quartz and CH.

Note in Figure 2b that there is a finite temperal witdth of the observed quartz-CH interface; this is the VISAR response time (given by the etalon thickness) are 60 and 170 ps. So the shock wave speed at the contact interface can not be measured directly. In order to obtain the shock velocity at the interface, we linearly fit the shock velocities

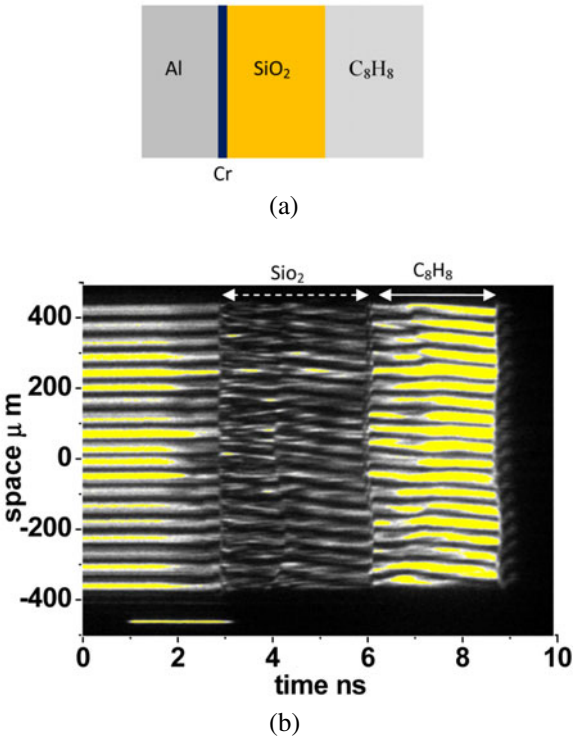

Fig. 2. (a) Schematic of the targets used in the experiments. (b) VISAR streak image, showing continuous track of shock front within standard and sample.

at least 0.3 ns before and after the interface transition region and extrapolates to the interface.

3 Principle of impedance-matching method

Shock pressures, densities, and specific internal energies were determined in all the experiments using the Rankine-Hugoniot jump conditions across a thin shock front [20]. These equations relate flow velocities and thermodynamic variables in the shocked state to those of the initial state:

$$P_1 - P_0 = \rho_0 U_S U_P \tag{1}$$

$$\rho_1 (U_S - U_P) = \rho_0 U_S \tag{2}$$

$$E_1 - E_0 = \frac{1}{2}(P_1 + P_0)\left(\frac{1}{\rho_0} - \frac{1}{\rho_1}\right) \tag{3}$$

where subscripts 0 and 1 denote initial and shock conditions in terms of pressure P, density ρ, and internal energy E. The first two equations have four unknowns (given that the initial pressure and density are known) and can be solved by measuring two variables. This solution constitutes a kinematic EOS and is often defined as U_S as a function of U_P. The high-pressure shock wave fronts are generally reflecting, and allowing one to measure the shock wave velocity using optical method, but it is difficult to measure the particle velocity directly. The

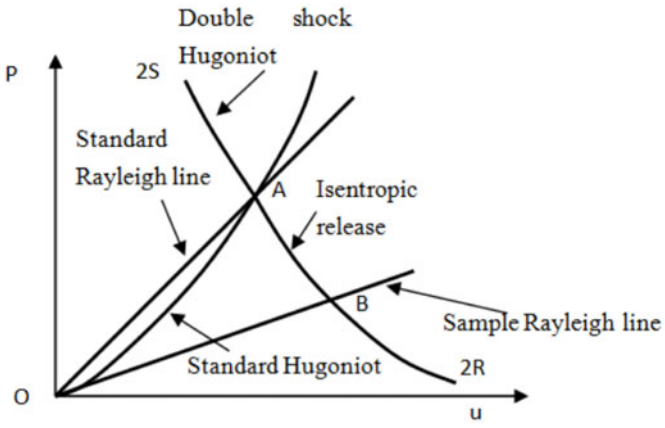

Fig. 3. Shock impedance match plot in P-U_P space.

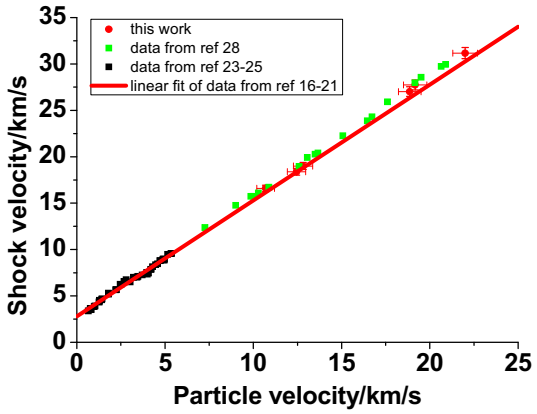

Fig. 4. Principal Hugoniot data for CH in the U_S-U_p plane. Data for this study were taken on Polystyrene (C_8H_8), with initial density $\rho_0 = 1.05$ g/cm^3, using IM with quartz standard.

principle of impedance-matching is pointed out so that the pressure and the particle velocity are conserved across the contact interface between the standard material and the sample. When the shock wave enters and exits the contact interface between the materials, the particle velocity can be deduced from the shock wave velocities in the standard and sample. This is shown in Figure 3 in the pressure-particle velocity (P-U_P) plane. By measuring the shock wave velocity in the standard material, the initial conditions of the shock wave before it interacts with the sample can be determined. This state (A) is the intersection of the Rayleigh line ($P = \rho U_S U_P$) and the known Hugoniot for the standard. If the impedance of the sample is higher than that of the standard, a shock wave will be reflected off the interface. If the impedance of the sample is less than the standard, a rarefaction wave will reflected off the interface. In any case, the continuity equation is satisfied at the interface between the standard and the sample. This determines the shocked state of the sample (Fig. 3). The second state in the sample is obtained by determining the first-shock states in both the standard and sample. By measuring two shock velocities in two materials (one in the standard and one in the sample), the particle velocity in the sample can be inferred. The sample EOS is defined by the U_S and U_P. One must make sure that the measured shock velocities are those just before and after the shock wave passing through the interface between the two materials. The shock wave jump conditions are derived from the mass and momentum the conservation. Under any condition, they are always satisfied regardless of shock planarity and stability. Therefore, shock steadiness is not a necessary condition for IM with transparent standards since jump conditions for a shock satisfied for decaying (and increasing) shock waves. If the shock velocity can be measured with sufficient time resolution, we can relax the requirement for shock steadiness as long as variation in velocity can be measured.

High precision principal Hugoniot of quartz was measured in the high-pressure fluid regime (200–1500 GPa) [21] using laser-driven shock waves. The quartz EOS is expressed by piecewise linear U_S-U_P relationship for the general form $U_S = a + bU_P$

$$U_S = 1.87 + 1.667U_P \tag{4}$$

$$U_S = 4.23 + 1.276U_P. \tag{5}$$

This U_S-U_P relation was used in this work. The quartz was shock to ∼300–1200 Gpa to produce reflective shock waves, the shock velocity was measured using VISAR, thereby determining the initial state of the standard for IM.

4 Shock adiabat of CH

Because the CH sample is transparent, we can provide high-precision EOS data by measuring the intantaneous velocities before and after the interface using the quartz as a standard. Several other precise IM measurements using quartz as standard have been demonstrated [22]. The continuity equations are central to the IM technique. As the shock passes through the boundary, the material accelerates, expands, and experiences shock, reshock, or release, to equilibrate and satisfy those conditions. The use of quartz standard and VISAR with high temporal resolution, High-precision shock velocities were obtained by providing "instantaneous" measurements. In this study, shock speeds were measured up to ∼1% precision. The shock velocities at the interface were determined by linear fitting over ∼300 ps before and after the quartz-sample interface and extrapolated to that interface.

Once velocities had been calculated the impedance match analysis was done by using the quartz EOS to find the state corresponding to the measured quartz shock velocity. The locus of the isentrope release state (for a release wave) in the pressure-particle-velocity plane originating from the reflected principal Hugoniot.

Figure 2b is an example of typical image obtained by the VISAR measurement. six shots were fired, and the results (Tab. 1) also shown in Figure 4 displays a U_S-U_P plot that also contains previous results [23–28].

Table 1. Polystyrene principal Hugoniot results from IM with quartz reference. Measured shock speed in the quartz and polystyrene, U_{SQ} and U_{SCH} is given. U_{PCH}, P_{CH} are the resulting particle velocity and pressure of shocked polystryrene obtained through the IM method.

No.	U_{SQ} (km/s)	U_{SCH} (km/s)	U_{PCH} (km/s)	P_{CH} (GPa)	
1	16.70 ± 0.34	18.38 ± 0.36	12.45 ± 0.52	240.24 ± 11.26	Big LA
2	14.96 ± 0.30	16.59 ± 0.34	10.70 ± 0.5	186.43 ± 9.4	Big LA
3	17.10 ± 0.34	19.00 ± 0.38	12.82 ± 0.54	255.65 ± 11.8	Big LA
4	26.68 ± 0.50	31.17 ± 0.60	22.00 ± 0.70	720.02 ± 27.24	Small LA
5	23.40 ± 0.46	27.02 ± 0.52	18.86 ± 0.64	534.98 ± 21.22	Small LA
6	23.77 ± 0.46	27.74 ± 0.54	19.17 ± 0.66	558.30 ± 22.0	Small LA

When the polystyrene is shock compressed to a few hundred GPa ranges, the temperature is likely to a few eV. At this pressure and temperature ranges, the polystyrene is likely to partially ionized, the electron distribution becomes partially degenerate. The polystyrene is likely to change from insulator to semiconductor.

5 Conclusion

High precision polystyrene equation of state data were measured using laser-driven shock waves with pressures from 180 GPa to 700 GPa. α quartz was used as standard material, the shock wave trajectory in quartz and polystyrene was measured using the Velocity Interferometer for Any Reflector (VISAR). Instantaneous shock velocity in quartz and polystyrene was obtained when the shock wave pass the interface. This provided $\sim$1% precision in shock velocity measurements.

References

1. A. Benuzzi, T. Löwer, M. Koenig, B. Faral, D. Batani, D. Beretta, C. Danson, D. Pepler, Phys. Rev. E. **54**, 2162 (1996)
2. D. Batani, A. Morelli, M. Tomasini, A. Benuzzi, F. Philippe, M. Koenig, B. Marchet, I. Masclet, M. Rabec, C. Reverdin, R. Cauble, P. Celliers, G. Collins, L. DaSilva, T. Hall, M. Moret, B. Sacchi, P. Baclet, B. Cathala, Phys. Rev. Lett. **88**, 235502 (2002)
3. D. Batani, F. Strati, H. Stabile, M. Tomasini, G. Lucchini, A. Ravasio, M. Koenig, A. Benuzzi, H. Nishinura, Y. Ochi, J. Ullschmied, J. Skala, B. Kralikova, M. Pfeifer, C. Kadlec, T. Mocek, A. Prag, T. Hall, P. Milani, E. Barborini, P. Piseri, Phys. Rev. Lett. **92**, 065503 (2004)
4. S.W. Hann et al., Phys. Plasmas **2**, 2480 (1995)
5. J.D. Lindl, Phys. Plasmas **2**, 3933 (1995)
6. T.R. Dittrich et al., Phys. Plasmas **6**, 2164 (1999)
7. C.E. Ragan III, Phys. Rev. A **25**, 3360 (1982)
8. A. Vladimirov, J. Exp. Theor. Phys. Lett. **39**, 82 (1984)
9. A.C. Mithcell, W.J. Nellis, J.A. Moriarty, R.A. Heinle, N.C. Holmes, R.E. Tipton, G.W. Repp, J. Appl. Phys. **69**, 2981 (1991)
10. M. Koenig et al., Appl. Phys. Lett. **72**, 1033 (1998)
11. M. Koenig et al., Phys. Plasmas **6**, 3296 (1999)
12. M. Koenig et al., Phys. Plasmas **12**, 012706 (2005)
13. R. Dezulian et al., Phys. Rev. E **73**, 047401 (2006)
14. F. Philippe et al., Phys. Plasmas **10**, 3026 (2003)
15. X.M. Deng, X.C. Liang, Z. Chen, Appl. Opt. **25**, 377 (1986)
16. S.Z. Fu et al., Phys. Plasmas **9**, 3201 (1995)
17. P.M. Celliers, D.K. Bradley, G.W. Collins, D.G. Hicks, T.R. Boehly, W.J. Armstrong, Rev. Sci. Instrum. **75**, 4916 (2004)
18. Shu Hua et al., Acta Physica Sinica **61**, 11410 (2012)
19. Shu Hua et al., Meas. Sci. Technol. **23**, 015203 (2012)
20. Jing Fu Qian, in *Introduction to experimental Equation of State* (Scientific Press, Beijing, 1999) pp. 204–210
21. D.G. Hicks, T.R Boehly., P.M. Celliers, J.H. Eggert, E. Vianello, D.D. Meyerhofer, G.W. Collins, Phys. Plasmas **12**, 082702 (2005)
22. D.G. Hicks et al., Phys. Rev. B **78**, 174102 (2008)
23. I.P. Dudoladov et al., Zh. Eksp. Eeor. Fiz. **4**, 148 (1969)
24. R.G. McQueen et al., in *High-Velocity Impact Phenomena* (Acdemic Press, New York, 1970), pp. 515–568
25. M. Van Thiel, Lawrence Livemore Laboratory Report UCRL-50108, Livermore, 1997
26. *LASL Shock Hugoniot Data*, edited by S.P. Marsh (University California Press, Berkeley, 1980), pp. 300–320
27. A.V. Bushman et al., Zh. Eksp.Teor. Fiz. **109**, 1662 (1996)
28. M.A. Barrios, D.G. Hicks, T.R. Boehly, D.E. Fratanduono, J.H. Eggert, P.M. Celliers, G.W. Collins, D.D. Meyerhofer, Phys. Plasmas **17**, 056307 (2010)